Photophysical Characteristics of Directly Linked Pyrene−Dimethylaniline Derivatives

S. Techert,*,† S. Schmatz,‡ A. Wiessner,† and H. Staerk*,†

Max-Planck-Institut für biophysikalische Chemie, Abteilung Spektroskopie und Photochemische Kinetik, Am Fassberg 11, D-37077 Göttingen, Germany, and Institut für Physikalische Chemie der Universität Göttingen, Tammannstrasse 6, D-37077 Göttingen, Germany

Received: October 5, 1999; In Final Form: January 28, 2000

Experimental and theoretical investigations of the spectroscopic properties have been carried out on three charge-transfer model systems, covalently linked donor−acceptor compounds of the type pyrene and derivatives of *N*,*N*−dimethylaniline (dimethyl(4-pyren-1-ylphenyl)amine (PyDMA), dimethyl(3-methyl-4-pyren-1-ylphenyl)amine (PyMDMA), and (3,5-dimethyl-4-pyren-1-ylphenyl)dimethylamine (PyDMDMA)). Comparing stationary absorption and emission spectra as well as fluorescence lifetimes in different solvents, one can show that small chemical changes such as substitution of ortho-hydrogens by methyl groups on the DMA moiety introduces dramatic effects in spectroscopic and kinetic behavior. On the basis of infrared measurements and quantum chemical calculations, the experiments are interpreted within a statistical framework, with particular emphasis on the discussion of preferred large amplitude motion (twist angle) and pyrene-specific vibronic coupling.

I. Introduction

Pyrene derivatives as partners in electron donor/acceptor systems have recently been introduced as fluorescence probes in biophysical chemistry. The fluorescence intensity and lifetime of pyrene can undergo significant changes upon hybridization of a covalently linked oligonucleotide to a DNA/RNA target strand and is used for sequence-specific detection of nucleic acids in solution.[1] Other examples of immediate interest are pyrene−aza-15-crown ether compounds that provide sensitive probes for the detection of metal ions in solution via the fluorescence and the magnetic field effect, respectively.[2,3] Quite another application is the utilization of one of the compounds (PyDMA), discussed in this report, in a charge-transfer dye laser, presently also in the form of a distributed feedback laser.

Since pyrene and derivatives, unlike other aromatic compounds, have turned out to be unique candidates for such studies, a profound and extended knowledge of their fundamental photophysicochemical properties (not available hitherto) is imperative, in protic as well as nonprotic solvents of varying polarity.

Since directly linked electron donor−acceptor systems have no extended bridge between the electron donor and acceptor moieties, the physical characteristics of these groups themselves strongly influence the mechanism of electron transfer. During the past decade several of such systems with varying donor/acceptor substitution have been studied. Focusing on peri-aromatic systems, in particular the systems with phenanthrene and anthracene as acceptor and dimethylphenylamine (DMA) as electron-donor shall be mentioned.[4−7]

E.g., in phenanthrene−DMA femtosecond transient absorption measurements show an intramolecular picosecond relaxation process of a "hot" charge-transfer species, which itself is generated within femtoseconds and decays either radiationless to a triplet state or fluoresces within nanoseconds.[4] Additionally, the solvent dependence of the fluorescence spectra cannot be explained within the so-called TICT (twisted intramolecular charge-transfer) model.[8] According to the TICT model, after light excitation a directly linked donor−acceptor system undergoes a radiationless adiabatic intramolecular electron transfer.[9−11] The reaction coordinate of the electron transfer is the torsional motion around the single bond that connects the electron donor and acceptor. In the so-formed TICT-state donor and acceptor are twisted 90° against each other, resulting in a high dipole moment. Because of solvent relaxation the TICT state can be stabilized.

Another system that has been studied is directly linked 9-anthracene−DMA (An−DMA), where the DMA moiety is substituted at the 9-position of anthracene.[5,6,12−14] (Polarized) stationary as well as kinetic measurements on this system show that the special behavior of 9-AnDMA can be explained by superposition of two different conformers: Calculations suggest that these conformers can mainly be distinguished by the dihedral angle between the phenyl moiety and the $N(CH_3)_2$ group. According to the absorption spectra, one of these conformers is thought to be formed through a ($\pi-\pi^*$) transition and the other conformer through direct absorption into a charge-transfer state with highly ionic character. Exciting in the blue-shifted ($\pi-\pi^*$) band (the locally excited state) the system undergoes a solvent-dependent fast relaxation to the charge-transfer state.

Compared to phenanthrene−DMA and anthracene−DMA, investigations of directly linked pyrene−DMA derivatives are scarce (see also ref 15). In this paper we report on the systems dimethyl(3-methyl-4-pyren-1-ylphenyl)amine (PyMDMA) and (3,5-dimethyl-4-pyren-1-ylphenyl)dimethylamine (PyDMDMA), which will be compared with dimethyl(4-pyren-1-ylphenyl)-amine (PyDMA), where pyrene and DMA can freely rotate relative to each other.[14,16] These compounds are shown in Figure 1. The only chemical difference in these charge-transfer (CT) systems is the ortho-substitution of methyl groups at the DMA moiety. Pyrene acts as the electron acceptor, whereas the

† Max-Planck-Institut.
‡ Universität Göttingen.

10.1021/jp9935384 CCC: $19.00
Published on Web 05/26/2000

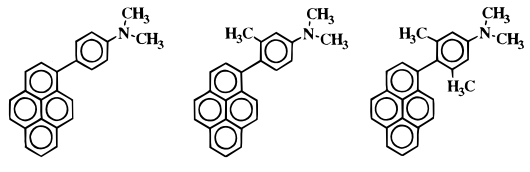

Figure 1. Structure of directly linked donor−acceptor systems studied in this work.

different covalently linked *N*,*N*-dimethylaniline derivatives are the electron donors.

In the present work special attention is paid to three facts that contribute to the complexity of the photophysics in PyDMA, PyMDMA, and PyDMDMA and explain why these compounds show such different behavior:

Twist Movement as Large Amplitude Motion. Looking at Figure 1 it is obvious, that the twist angle between electron donor (DMA and derivatives, respectively) and electron acceptor (pyrene) will differ due to steric hindrance. The difference in the twist angle influences the electronic coupling between the moieties and therefore the spectroscopic and kinetic properties. Also the positive inductive effect of the methyl moieties on the electron donor changes the redox properties of the system, which influences the charge-transfer characteristics. From previous experiments on free systems one knows that every additional CH_3 group on the phenyl ring leads to a lowering of the oxidation potential by approximately 0.08 eV.[17] Since until now the geometries of charge-transfer states cannot be directly experimentally determined, indirect approaches such as quantum chemical calculations have to be introduced in the discussion about dihedral angles between electron donor and acceptor etc. Furthermore, the resulting physical properties such as dipole moments have to be compared with the experimental data.

Statistical Approach. Nevertheless, as pointed out in the work on a similar system (phenanthrene−DMA),[4] twist angle and redox potential alone cannot explain the behavior especially of PyDMA. To get a more detailed understanding of the systems, the absorption spectra/absorption coefficients of the CT compounds are analyzed in a full statistical approach, which considers all internal degrees of freedom in the molecule and not only the twist motion between electron donor and electron acceptor. Further, from the statistically weighted absorption coefficients or oscillator strengths, respectively, the emission lifetimes can be calculated. To do so, infrared measurements were carried out and the assigned vibrations, each of which represents one internal degree of freedom, were included in the analysis of the absorption spectra and the CT lifetimes. The IR measurements were supplemented by quantum chemical simulations.

Vibronic Coupling. Pyrene as a periaromatic molecule shows a characteristic vibronic coupling that influences absorption and emission properties and will ultimately be mentioned.

Much work (e.g., the cited references), which deals with the influence of additional substitution on photophysical properties of donor and acceptor, respectively, explains the different behavior with redox potential properties and large amplitude twist motion (point one of the above list). Though these points are doubtless essential for the understanding of the properties of such compounds, it may not be sufficient to understand the physical behavior on a higher level of spectroscopic interpretation like the consideration of all degrees of freedom in a molecule or special spectroscopic features, e.g., vibronic couplings. Therefore, the aim of this paper is, after reflecting and discussing the common way of explaining the different properties of PyDMA, PyMDMA, and PyDMDMA by comparing experimental results with quantum chemical calculations, to enlarge the discussion on points, which until now are not sufficiently considered in the literature (namely, the statistical analysis of the absorption and emission spectra/lifetimes and the extraction of pyrene-characteristic vibronic coupling).

This paper is organized as follows: In chapter II the experimental details are reported. In chapter III the results and a detailed discussion are presented. Our conclusions are drawn in section IV.

II. Experimental Section

A. Synthesis and Sample Preparation. After the diazotation of 1-aminopyrene[18] it was coupled to either *N*,*N*-dimethylaniline, *N*,*N*-dimethyl-*m*-toluidine, or *N*,*N*-3,5-tetramethylaniline according to a literature method.[19] The crude compounds were purified on an aluminum oxide column using a mixture of cyclohexane/toluene as eluting solvent and applying HPLC. The compounds were identified by mass spectrometry (Varian CH7, 70 eV) [*m*/*e* (relative intensity): PyDMA, 321 (M^+, 100); PyMDMA, 335 (M^+, 100); PyDMDMA, 349 (M^+, 100)] and ^{1}H NMR measurements (Bruker 80 MHz, $CDCl_3$, TMS = internal reference) [PyDMA: $N(CH_3)_2$, 3.05 (s, 6H); phy-H, 6.9 (d, 2H); phy-H, 7.55 (d, 2H); pyrene-H 7.8−8.4 (m, 9H). PyMDMA: phy-CH_3, 2.05 (s, 3H); $N(CH_3)_2$, 3.05 (s, 6H); phy-H_4, 6.8 (d, (+ m-coup.), 1H); phy-H_3, 6.77 (s (+ m-coup.), 1H); phy-H_5, 7.30 (d, 1H); pyrene-H 7.8−8.4 (m, 9H). PyDMDMA: phy$(CH_3)_2$, 1.9 (s, 6H); $N(CH_3)_2$, 3.05 (s, 6H); phy-H_5, 6.75 (s, 2H); pyrene-H 7.6−8.4 (m, 9H)].

The solvents used for the experiments were of spectroscopic grade: *n*-hexane (Merck), several *n*-alcohols with increasing number of chain carbons (Fluka) and acetonitrile ACN (Merck).

The samples were degassed by applying freeze−pump−thaw cycles. The concentrations of the sample solutions were on the order of 10^{-5} M. To exclude saturation effects, the concentrations of the solution were optimized either on the absorption maxima of the spectra or on the wavelength of interest, so that the optical density OD was 0.5−1.0 in a 1 cm thick cuvette.

B. Methods and Apparatus. The stationary absorption spectra have been measured with a Cary-5E spectrometer. A Perkin-Elmer LS50 fluorescence spectrometer was used in order to record the stationary fluorescence spectra; these were quantum-corrected after the measurements. For the fluorescence quantum yield measurements ca. 0.1 N quinine bisulfate (CBS) in sulfuric acid (with a quantum yield of $\Phi(\mathrm{CBS}) = 0.51$) was used as the reference compound.[20] All solutions including quinine bisulfate were excited at 337 nm. The quantum yield was calculated according to standard procedures.[21] In the determination of the quantum yield the various optical densities as well as the changes of the refractive index of the different solvents have been considered.

In the wavelength range between 250 and 700 nm the bandpass of the UV absorption and emission spectrometer was 0.5 and 2 nm, respectively, resulting, e.g., in a resolution of about 55 cm^{-1} at 350 nm in emission. UV absorption and emission spectroscopy have been complemented by spectroscopic measurements with polarized light using broadband polaroid filters (between 50% and 70% transmission) in a refractometer-like arrangement.

The infrared measurements were carried out using a Fourier transform infrared spectrometer (Bruker 5-HR). The resolution of the FTIR spectrometer was 0.5 cm^{-1}. The measurements covered an area between 600 and 3500 cm^{-1}.

In the nanosecond range the fluorescence decay curves were recorded with a standard time-correlated single photon counting apparatus (Edingburgh Instruments, 0.5 ns resolution) with a nitrogen flashlamp as excitation source. The 337 nm emission of nitrogen was used for sample excitation. The data were analyzed using a deconvolution technique and fitted with a nonlinear least-squares fitting method based on the Levenburg−Marquardt algorithm to mono/multiexponential decay laws such as $\sum_i A_i \exp(-t/\tau_i)$. The accuracy was ±0.2 to ±0.5 ns corresponding to a relative accuracy of ±2% at 20 ns (with $\chi^2 \simeq 1.1$).

All measurements were carried out at $T = 25$ °C using a thermally controlled sample holder.

III. Results and Discussion

The three points, on which this paper focuses, "twist movement as large amplitude motion", "statistical approach/analysis", and "pyrene-characteristic vibronic coupling", are discussed in the subsections of this chapter:

In subsections IIIA and IIIB we report on the stationary absorption and emission spectra of PyDMA, PyMDMA, and PyDMDMA. In subsection IIIC these spectra are compared with results from ab initio calculations on CT properties. In subsection IIID a statistical vibrational analysis of the ground and excited states has been performed on the basis of IR measurements and applied to the absorption and emission spectra. Subsection IIIE discusses the experimental results with particular emphasis on the influence of vibronic coupling and densities of vibrational states on the CT processes.

A. Stationary Absorption Spectra. Figure 2 shows the normalized absorption spectra of PyDMA (top), PyMDMA (middle), and PyDMDMA (bottom) in solvents with strongly varying permittivity. These solvents are *n*-hexane with a permittivity $\epsilon_S = 1.9$, hexanol with $\epsilon_S = 13.0$, and ACN with $\epsilon_S = 37.5$.

How the difference in chemical substitution on the electron donor moiety influences the spectral behavior can best be seen starting with PyDMDMA at the bottom of Figure 2. Here, the absorption spectrum of PyDMDMA in different solvents is compared with the absorption spectrum of 1-methylpyrene in hexOH: PyDMDMA is a doubly substituted system, where the DMDMA moiety is nearly 90° twisted against the pyrene plane due to steric hindrance (see also results of calculations, subsection IIIC). The twist leads to an electronically decoupled system, since the π-orbitals of the aromatic systems of the pyrene and phenyl moieties stay nearly perpendicular to each other. Therefore, the absorption spectrum of PyDMDMA is of all the three observed systems the one most similar to the absorption spectrum of pyrene or, more realistically, 1-methylpyrene. Since 1-methylpyrene has the same symmetry elements as PyDMDMA (C_s point group), PyDMDMA follows essentially the same optical selection rules as 1-methylpyrene: The first electronic transition (around 370 nm) is forbidden for 1-methylpyrene as well as for PyDMDMA (for the detailed assignment of pyrene or pyrene derivative spectra, see refs 22−25).

In the region of the transition of the second excited state (higher than 350 nm) the UV absorption spectrum of pyrene or 1-methylpyrene is characteristically dominated by the occurrence of four to five vibrationally resolved features.[23,24] For the most part this pattern remains in the case of PyDMDMA, though the vibrationally resolved transitions belonging to the $S_1 \leftarrow S_0$ transition (around 370 and 355 nm) are smeared out; the S_1 state seems to have some charge-transfer character.

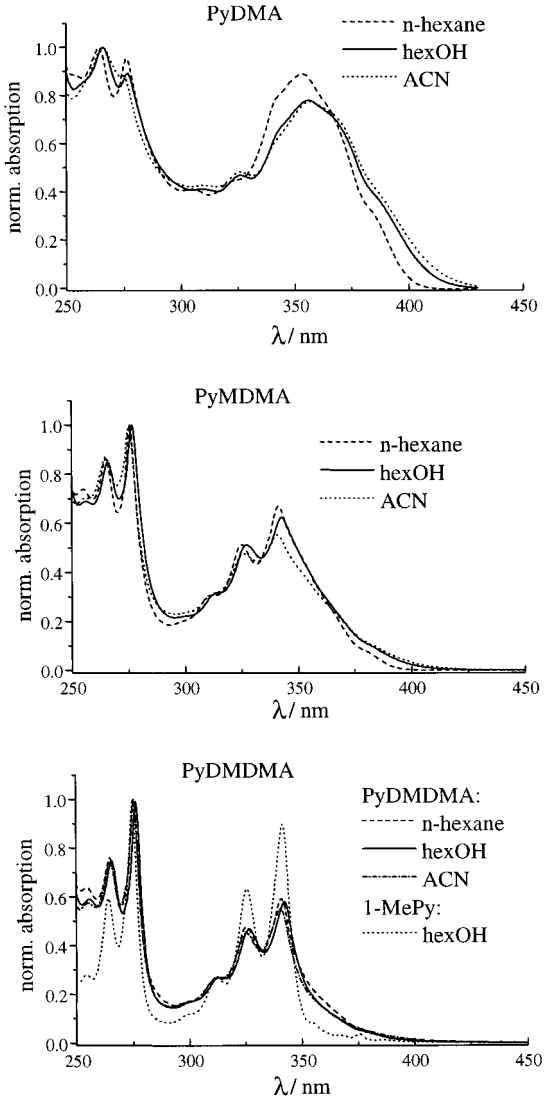

Figure 2. Normalized stationary absorption spectra of PyDMA (top), PyMDMA (middle), and PyDMDMA/1-methylpyrene (bottom) in three different solvents (*n*-hexane, hexanol, and ACN).

For different solvents the absorption spectra of PyDMDMA differ, but not significantly, from each other.

If one methyl group is removed (see PyMDMA, the middle of Figure 2), the twist between the DMA moiety and the pyrene moiety is not as rigid as in PyDMDMA anymore and an additional absorption band smoothly grows out of the low energy side of the absorption band. As in PyDMDMA the absorption spectra are nearly solvent-independent.

In the case of PyDMA, where both methyl substitutions are removed, the additional absorption band is dramatically increased and strongly superimposes with the characteristic vibrationally resolved spectrum of pyrene to a broadly smeared out absorption band. Obviously, the intensity of the additional absorption band is dependent on the freedom of twist between the DMA and pyrene moieties and therefore on the strength of the electronic coupling between pyrene and DMA. For PyDMA the angle of the twisting motion is on the order of 65° (see chapter IIIC), which leads to a larger electronic coupling between the moieties.

For different solvents the absorption spectra are slightly shifted against each other. The nonnegligible solvent dependence of the absorption band of PyDMA (see also refs 14 and 26) is an indication that the band belongs to a transition from the

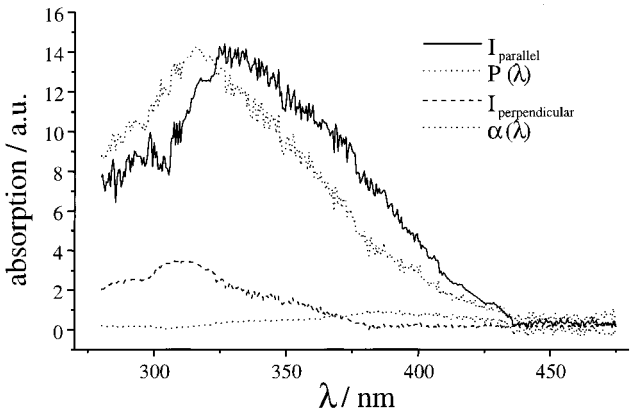

Figure 3. Polarization absorption spectrum of PyDMA in stretched polyethylene foil.

electronic ground state directly into a CT state. In PyMDMA and PyDMDMA the S_1 has also CT character (broad band around 370 nm), though not as pronounced as in PyDMA.

The polarization absorption spectrum of PyDMA on stretched polyethylene (PE) foil is shown in Figure 3. The spectrum clearly shows parallel as well as perpendicularly polarized components, which also support the interpretation of an optically generated charge-transfer state. The degree of anisotropy of the absorption spectrum is nearly wavelength-independent.

The polarization spectrum was calculated according to[27]

$$P(\tilde{\nu}) = \frac{I_{||}(\tilde{\nu}) + 2I_{\perp}(\tilde{\nu})}{3} \quad (1)$$

and the degree of anisotropy of the spectrum according to

$$\alpha(\tilde{\nu}) = \frac{I_{||}(\tilde{\nu}) - I_{\perp}(\tilde{\nu})}{I_{||}(\tilde{\nu}) + 2I_{\perp}(\tilde{\nu})} \quad (2)$$

Since stretched PE foil was used as the orientation medium, the molecules are not strongly anisotropically aligned. Therefore, the measured parallel and perpendicular intensities have to be weighted with the factors $K_{||} = 0.63$ and $K_{\perp} = 0.29$.

B. Stationary Emission Spectra and Fluorescence Lifetimes. In Figure 4 the normalized emission spectra of PyDMA in *n*-hexane, hexanol, and ACN are displayed in the top, the spectra of PyMDMA in the same solvents in the middle and the spectra of PyDMDMA in the bottom panel. All three compounds show large bathochromic shifts (cf. Table 1). The shifts are dependent on the redox properties and on the dipole moment of the CT species; this, obviously, also as a consequence of the strength of the electronic coupling. E.g., in the case of PyDMA in hexanol the Stokes shift of the band relative to the one in the nonpolar solvent *n*-hexane is $\Delta\tilde{\nu}_{max}$(PyDMA) $\simeq 2700$ cm^{-1}. For the monosubstituted PyMDMA the emission band shifts further to the red with $\Delta\tilde{\nu}_{max}$(PyMDMA) $\simeq 4200$ cm^{-1}. In the bisubstituted system PyDMDMA the Stokes shift is maximal with $\Delta\tilde{\nu}_{max}$(PyDMDMA) $\simeq 5700$ cm^{-1} (Table 1).

Also due to the inductive effect of the methyl groups, the donor ability of the DMA moiety increases by 0.08 eV for each additionally substituted methyl group. Therefore, the redox potential between electron donor and acceptor decreases and the CT band shifts bathochromically.

In the various solvents all three systems show only one broad emission band, which can be assigned to a charge-transfer fluorescence. No vibrationally structured emission from a locally excited (LE) state could be found. The polarization spectrum

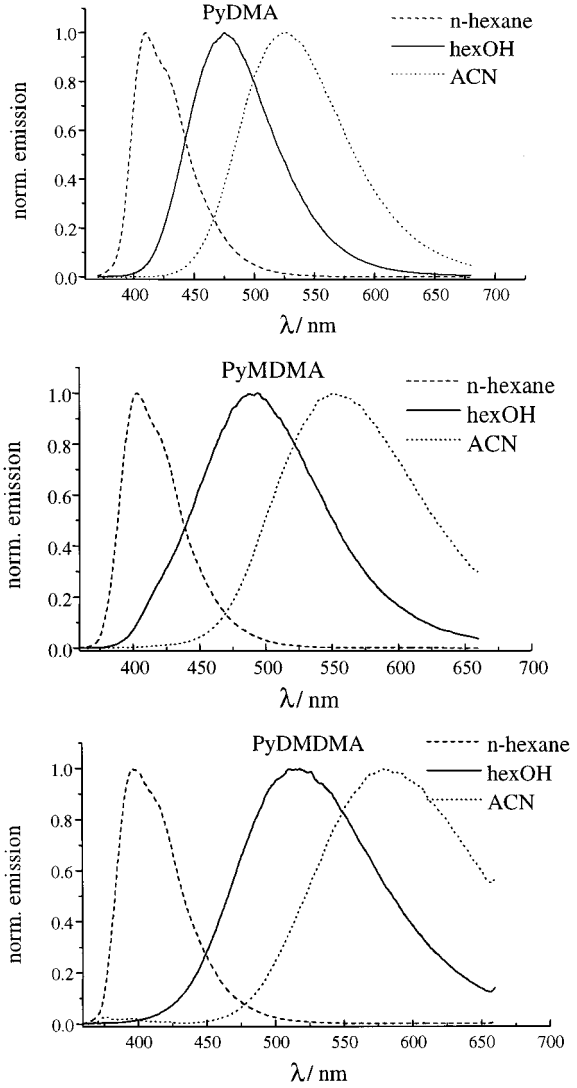

Figure 4. Normalized stationary emission spectra of PyDMA (top), PyMDMA (middle), and PyDMDMA (bottom) in *n*-hexane, hexanol, and ACN.

of PyDMA in stretched polyethylene (PE) foil is shown in Figure 5. As in the case of the absorption spectra, the emission band shows parallel as well as perpendicularly polarized components. The polarization spectrum in emission were treated in the same way as the absorption spectra. Also here the degree of anisotropy of the emission spectrum is wavelength-independent.

Table 1 summarizes the main stationary and kinetic features of the charge-transfer emission of PyDMA, PyMDMA, and PyDMDMA. For the determination of the band maximum $\tilde{\nu}_{max}$ and the full width at half-height $\Delta\tilde{\nu}_{FWHH}$ as fit function for the charge-transfer band the "log-normal" function was used. Both the band maximum and the FWHH show a strong solvent dependence. For PyDMA the quantum yields of the CT species, Φ_{CT}, are near unity and show only slight solvent dependence. The quantum yield for PyMDMA extends from 1 to 0.8 and for PyDMDMA from 0.8 to 0.4 with increasing solvent polarity.

In the case of PyDMA kinetic parameters such as the CT lifetimes increase with increasing solvent polarity. PyMDMA and PyDMDMA follow the opposite trend. The lifetimes τ_{CT} of the stabilized CT species range from 3 to 7 ns for PyDMA, from 4 to 15 ns for PyMDMA and from 12 to 25 ns for PyDMDMA. The fluorescence rate constants calculated accord-

TABLE 1: Main Stationary and Kinetic Features of the Charge-Transfer Emission Spectra of PyDMA,[14] PyMDMA, and PyDMDMA[a]

substance	solvent	ϵ_S	$\tilde{\nu}_{max}/cm^{-1}$	$\Delta\tilde{\nu}_{FWHH}/cm^{-1}$	Φ_{CT}	τ_{CT} [b]/ns	$\kappa_{CT}/10^8\ s^{-1}$	$\langle n^3\tilde{\nu}^3\rangle/10^{13}\ cm^{-3}$	$\kappa_{CT}/10^{-6}\ s^{-1}\ cm^{-3}$
PyDMA	*n*-hexane	1.89	23520	2951	0.82	2.5	3.23	3.35	9.7
	etoac	6.02	20830	3390	0.92	3.9	2.36	2.25	10.5
	hexOH	13.0	20805	3753	0.97	3.7	2.62	2.44	10.7
	pentOH	14.8	20600	3750	0.89				
	propOH	20	20200	3815	0.97				
	etOH	25	19700	3900	0.91				
	meOH	32.6	19420	3970	0.88				
	ACN	37.5	18776	*3757	0.95	6.5	1.46	1.60	9.1
PyMDMA	*n*-hexane	1.89	24430	3026	0.98	4.4	2.23	3.54	6.3
	octOH	10.3	20400	4372	0.87	7.6	1.14	2.44	4.7
	hexOH	13.0	20027	4735	0.82	8.3	0.99	2.33	4.3
	ACN	37.5	17692	*4257	0.81	15.4	0.53	1.42	3.73
PyDMDMA	*n*-hexane	1.89	24724	3088	0.78	12.4	0.63[c]	3.65	1.73[c]
	etoac	6.02	19625	4217	0.75				
	octOH	10.3	19155	4476	0.62	19.6	0.32[c]	2.11	1.50[c]
	hexOH	13.0	18983	4586	0.65	20.2	0.32[c]	1.99	1.61[c]
	pentOH	14.8	18850	4706	0.48				
	ACN	37.5	16740	*4253	0.41	24.4	0.17[c]	1.29	1.32[c]

[a] * Denotes the bandwidth from strongly approximated emission bands in the red region of the spectrum, which could not be fully quantum corrected. [b] Lifetime of the stabilized CT species. [c] The more complex mechanism of PyDMDMA requires a more detailed consideration in conjunction with picosecond data.[28] The numbers for k_{CT} and κ_{CT} are therefore too small by 2−4%.

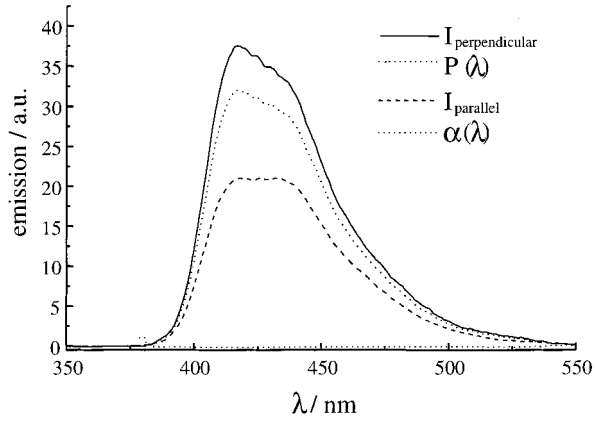

Figure 5. Polarization emission spectrum of PyDMA in stretched polyethylene foil.

ing to $k_{CT} = \Phi_{CT}/\tau_{CT}$ also reflect this difference in the behavior of PyDMA compared to PyMDMA and PyDMDMA in the different solvents. Since the emission probability depends on the wavelength,[22] for a physically correct comparison the $n^3\tilde{\nu}^3$ correction has to be applied according to the equations:

$$\kappa = \frac{k_{CT}}{\langle n^3\,\tilde{\nu}^3\rangle} \tag{3}$$

$$\langle n^3\,\tilde{\nu}^3\rangle = n^3\,\frac{\sum_i I_i(\tilde{\nu}_i)\tilde{\nu}_i^{\,3}}{\sum_i I_i(\tilde{\nu}_i)} \tag{4}$$

where $\langle n^3\tilde{\nu}^3\rangle$ is the band-averaged correction factor and $I_i(\tilde{\nu}_i)$ the fluorescence intensity at wavenumber $\tilde{\nu}_i$.

Focusing on the κ values (3), the solvent dependence of the lifetimes can be explained as follows: For PyDMA, within the experimental uncertainity of the photon counting measurements the increasing lifetime can satisfactorily be explained by the frequency-dependent emission probability, since the κ values are solvent-independent. The oscillator strength remains virtually unchanged, which suggests that in PyDMA no coupling between the intramolecular motion (this affects the oscillator strength) and the solvation coordinate exists. This behavior changes in PyMDMA, where even with the applied correction (3) κ decreases with increasing solvent polarity. Since the κ values are proportional to the square of the transition dipole moment, the results suggest that in PyMDMA a coupling exists between an intramolecular motion, which affects the oscillator strength and the solvent coordinate. More difficult is the interpretation of the κ values in PyDMDMA: According to Table 1 the κ values seem to be solvent-independent—at least within the time resolution of the photon counting apparatus and applying equation $k_{CT} = \Phi_{CT}/\tau_{CT}$ for the rate constant calculation. That this result has to be slightly relativized if one goes to picosecond time resolution will be shown in ref 28. Since the fluorescence spectra of all three substances in ACN extend across the wavelength range of the quantum correction with limit at about 650 nm, the emission bands are strongly approximated beyond this wavelength and lead possibly to an underestimation of the quantum yield in ACN.

To determine the dipole moments of the charge-transfer species of PyDMA and PyDMDMA the equation

$$\tilde{\nu}_{max} = \tilde{\nu}^0_{max} - \frac{2\mu^2}{hc\rho^3}\left[f(\epsilon_s,n) - \frac{1}{2}f'(\epsilon_s,n)\right] \tag{5}$$

was used.[29−33] In eq 5 the gradient of the CT emission band maximum $\tilde{\nu}_{max}$ with respect to the solvent factor $f(\epsilon_s,n) - {}^1/_2 f'(\epsilon_s,n)$ is proportional to the dipole factor μ^2/ρ^3, as plotted in Figure 6. Depending on the shape of the dipole (spherical or cylindrical shaped) the solvent factor $f(\epsilon_s,n) - {}^1/_2 f'(\epsilon_s,n)$ has to be determined according to

$$f(\epsilon_s,n) - \frac{1}{2}f'(\epsilon_s,n)\ (\text{sphere}) = \frac{\epsilon_s - 1}{\epsilon_s + 2} - \frac{n^2 - 1}{2n^2 + 1} \tag{6}$$

$$f(\epsilon_s,n) - \frac{1}{2}f'(\epsilon_s,n)\ (\text{cylinder}) = \frac{\epsilon_s - 1}{2\epsilon_s + 1} - \frac{n^2 - 1}{2n^2 + 1} \tag{7}$$

With an estimated molecular volume of about $V_{molec} = \rho_{molec}{}^3 \simeq 7^3$ Å^3 to $\rho_{molec}{}^3 \simeq 9^3$ Å^3 the slope of the plots lead to dipole moments of the CT species of about μ(PyDMA) = 21−22 D, μ(PyMDMA) = 24 D, and μ(PyDMDMA) = 25−26 D. The limitation of this way of dipole moment determination is based on the classical treatment of the solvent as a dielectric continuum

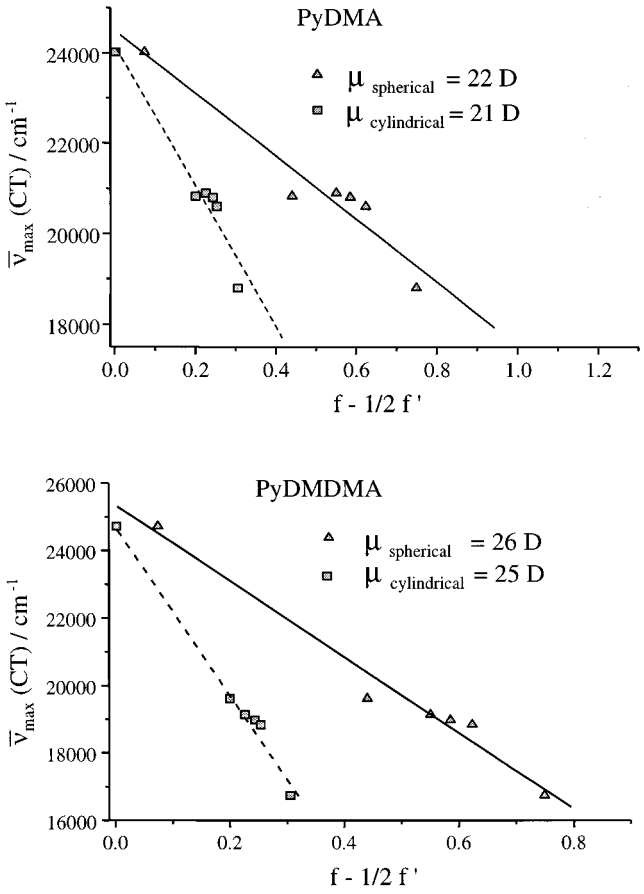

Figure 6. Determination of the dipole moment of the charge-transfer species of PyDMA (top) and PyDMDMA (bottom) according to eq 5.

as well as on the treatment of the molecule as a point dipole in the center. Including the correction for a cigar-shaped dipole, which describes more realistically the charge distribution in PyDMA/PyDMDMA, the numbers for the dipole moment slightly but not dramatically improve. Also, it should be pointed out that eq 5 originally has been derived for sandwich like donor/acceptor complexes. The estimated error for the dipole moment is therefore on the order of 20%.

C. Ab Initio Calculations of the Charge-Transfer State: Twist in Geometry and Electron Donor−Acceptor Capabilities. Ab initio calculations yield further indication for an optical electron transfer in the observed systems. The calculations were carried out on PyDMA and PyDMDMA using the Gaussian 94 suite of programs.[34] The 6-31G basis set was used for the restricted Hartree−Fock (RHF) calculations of the ground-state geometries. The optimized geometries show intramolecular dihedral angles of Θ(py−dma) ≃ 64° for the pyrene/DMA moieties of PyDMA and a dihedral angle of Θ(py−dma) ≃ 90° in the case of PyDMDMA. PyMDMA has a dihedral angle of about 79°.

In further calculations the intramolecular dihedral angles Θ(py−dma) were fixed at 64° and at 90° for PyDMA and at 90° for PyDMDMA. The excited electronic states at the different geometries and their properties such as the oscillator strengths were calculated with the configuration interaction with single (CIS) method,[35] which often causes problems with the ordering of states calculated for the gas phase.[8,36] Responsible for these artifacts is mainly the lack of static and dynamic electron correlation effects, which are included in more sophisticated methods such as MC-SCF/CASSCF or MRCI. However, these methods are computationally more demanding, and even with a low-quality one-particle basis set, calculations on the systems studied in this work are unfeasible at present.

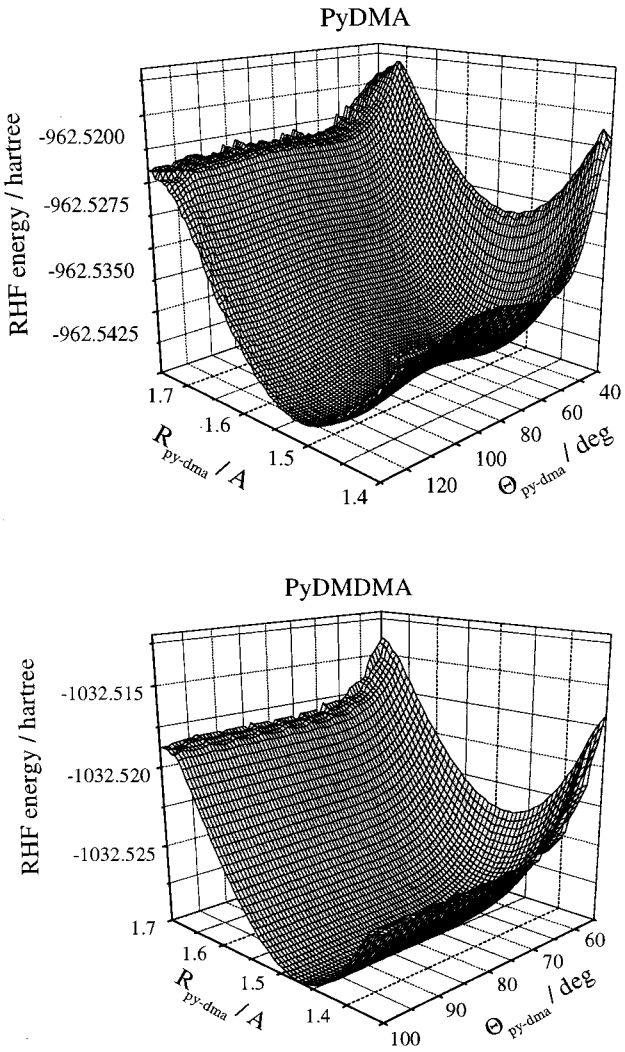

Figure 7. Potential energy surface of the ground state of PyDMA including the anharmonic motion (top) and potential energy surface of the ground state of PyDMDMA (bottom). R_{py-dma} is the bond length between pyrene and DMA and Θ_{py-dma} is the dihedral angle between these two moieties.

Figure 7 shows the potential energy surface (PES) of PyDMA as a function of the dihedral angle Θ_{py-dma} and the bond length R_{py-dma}. The strongly anharmonic double-well torsional potential leads to a splitting of the vibrational states, which influences the statistical treatment of the kinetics (see IIID). For the ground state of PyDMA, the potential energy barrier V_0^{calc} at 90° is only 20−30 cm^{-1} high. V_0^{calc} increases for the first excited (CT) state to about 500 cm^{-1}. In the second excited state V_0^{calc} amounts to 200 cm^{-1}. Also displayed in Figure 7 is the PES of PyDMDMA, which shows a single minimum around Θ_{py-dma} = 90°. As expected, the py−dma bond length increases with methyl substitution (from 1.4935 Å (PyDMA) to 1.5148 Å (PyMDMA) and 1.5161 Å (PyDMDMA)). The sp^3 character of the amino nitrogen slightly increases from PyDMA to PyDMDMA. In the case of PyDMDMA the center of mass of the amino moiety is located about 5° out of the phenyl plane, whereas it lays in the plane in the case of PyDMA and PyMDMA.

If one compares the bond lengths and angles obtained using ab initio calculations with results from semiempirical methods such as AM1, the ab initio values are in general larger by 2%,

TABLE 2: Ab Initio Calculations of Some Physical Properties of PyDMA and PyDMDMA in Different Electronic States (for Details, See Text)

substance	state	Θ(py−dma)/deg	μ^{obs}/D	μ^{calc}/D	f_{osc}^{obs}	f_{osc}^{calc}	τ^{obs}/ns	τ^{calc}/ns	τ^{calc}(HexOH)/ns
PyDMA	ground state	64		2.2					
		90		2.3					
	S_1	64	22	12	0.320	0.725	3.7	2.7	3.1
		90		22		0.016		110	197
	S_2	64		2	1.000	0.883			
		90		2		0.034			
PyDMDMA	ground state	90		2			20.2	37	78
	S_1	90	26	25	0.014	0.04			
	S_2	90		2	0.900	0.31			

even by 10% for all anharmonic intramolecular coordinates such as the dihedral angle Θ_{py-dma}. The agreement with the experimental data (vibrational frequencies as well as dipole moments or oscillator strengths, see Table 2) is satisfactory.

To compare the calculations with experiment, vibrational effects should also be included, e.g., for the transition $S_x^{\upsilon=0} \leftarrow S_0^{\upsilon=0}$ the difference of the zero-point energies in both electronic states. Because of the remarkably large number of vibrations (126 for PyDMA, 135 for PyMDMA, and 144 for PyDMDMA) huge zero-point vibrational energies such as G_{zp}(PyDMA) $\simeq$ 72 020 cm^{-1}, G_{zp}(PyMDMA) $\simeq$ 74 560 cm^{-1}, and G_{zp}(PyDMDMA) $\simeq$ 81 040 cm^{-1} are obtained. Thus, relatively small changes in the shape of the excited PES's compared to the ground-state PES lead to small changes in every fundamental wavenumber, but summed up may yield not negligible differences in the zero-point energies of an excited PES and the ground-state PES. Assuming, e.g., for a CT transition a change of 5% in all vibrational frequencies, the neglect of the difference between the zero-point energies in the worst case can result in an error of the energy on the order of about 10 nm or even more for an electronic transition at 400 nm. Since in PyDMA, PyMDMA, and PyDMDMA the shape of the band, which belongs to the transition in the CT state is relatively broad, the transition seems to lead to a repulsive region on the excited PES.[37] Thus, it is quite reasonable to assume that the fundamental wavenumbers of the first excited state differ from the corresponding quantities in the ground state (assumed: 5%). Since the transitions into the second electronically excited-state preserve the characteristic pyrene spectrum, the second excited state is a Franck−Condon state with a geometry comparable to the geometry of the ground state. Therefore, for the second excited PES a change of the fundamental vibrational wavenumbers of 1% was assumed. Taking all these corrections into account the $S_1 \leftarrow S_0$ and $S_2 \leftarrow S_0$ transition energies of PyDMA are calculated to $\tilde{\nu}^{calc}(S_1,S_0) = 33\,179$ cm^{-1} (4.1 eV) and $\tilde{\nu}^{calc}(S_2,S_0) = 37\,456$ cm^{-1} (4.6 eV). In *n*-hexane the measured term values are $\tilde{\nu}^{obs}(S_1,S_0) = 25\,776$ cm^{-1} (3.2 eV) and $\tilde{\nu}^{obs}(S_2,S_0) = 28\,938$ cm^{-1} (3.6 eV). Similar results are obtained for PyDMDMA. The calculated energies $\tilde{\nu}^{calc}(S_1,S_0) = 35\,343$ cm^{-1} (4.4 eV) and $\tilde{\nu}^{calc}(S_2,S_0) = 36\,337$ cm^{-1} (4.5 eV) are comparable with the measured ones in *n*-hexane ($\tilde{\nu}^{obs}(S_1,S_0) = 26\,441$ cm^{-1} (3.3 eV) and $\tilde{\nu}^{obs}(S_2,S_0) = 29\,317$ cm^{-1} (3.6 eV)). Though the above-mentioned corrections lead for PyDMA and PyDMDMA to the right order of the excited states, calculated and measured values differ on the order of 25%, which is far too high.

Even if the energetic results from HF/CIS calculations may be difficult to judge, geometries, dipole moments, and oscillator strengths can be calculated with acceptable accuracy using the HF method. In Table 2 these properties are listed for the ground and the first and second excited states of PyDMA and PyDMADMA and compared with results from stationary spectra.

For all electronic states the dipole moments were calculated using the HF method. For the first excited state the calculated dipole moment of PyDMDMA nicely agrees with the experimentally determined quantity. For PyDMA the corresponding dipole moment is obtained 45% too small for the 64° configuration but exact for the 90° configuration. However, it should be kept in mind that the determination of the dipole moment in the excited-state according to eq 5 is not unambigious and errors of $\Delta\mu = 20\%$ should be considered for PyDMA, PyMDMA, and PyDMDMA.

For PyDMA the calculated oscillator strengths come out to the same order of magnitude for the 64° configuration and one order of magnitude too low for the 90° configuration compared to the experimental data. For the second excited state the oscillator strength at the 64° configuration agrees well with the experimental result. In PyDMDMA the calculated oscillator strengths are in the same order of magnitude, but too big for the first and too small for the second excited state.

Calculated and measured lifetimes are compared in Table 2 where τ^{calc} denotes the lifetimes, directly determined from the oscillator strengths f_{osc}^{calc}. Since these data were obtained for the gas phase, some solvent stabilization terms have to be included for a comparison of lifetimes measured in solution. For the determination of the solvent stabilization the calculated dipole moments and term values were inserted in eq 5 and the solvent-stabilized term value $\tilde{\nu}_{max}$ was recalculated and used in eq 9. Equation 9 will be further explained in detail in the following section. In the case of PyDMA and at the 64° configuration the lifetimes determined in the way described match the measured lifetimes within 72% without solvent correction and within 84% with solvent correction. Obviously, in the solvent correction the too small calculated dipole moment compensates the too big calculated oscillator strength. For the 90° configuration the calculated lifetimes are far off even with solvent correction. However, the theoretical results in general match the measured properties within the same order of magnitude. The comparison of theoretical and experimental results show that a pure 90° configuration of PyDMA cannot explain the experimental behavior.

Since in PyDMDMA the oscillator strength is too large for the first excited state, the lifetime from ab initio calculations comes out too big with an error of about 46%. The extremely high dipole moment of PyDMDMA leads to an enormous solvent stabilization, which results in a lifetime shift of τ_{calc}(gas) − τ_{calc}(HexOH) = 41 ns, which is surprisingly far off and not explainable by the difference in the oscillator strengths. The difference can only be explained by the occurrence of an additional radiationless reaction channel or by the solvent-assisted generation of a radical ion pair, which is not the subject of the calculations in this chapter (see ref 28).

To understand the charge distribution of PyDMA, PyMDMA, and PyDMDMA in the ground state and in the excited electronic states, a Mulliken population analysis[38] was performed. The results are graphically displayed in Figure 8. Full circles assign the center of positive charge, and open circles denote centers

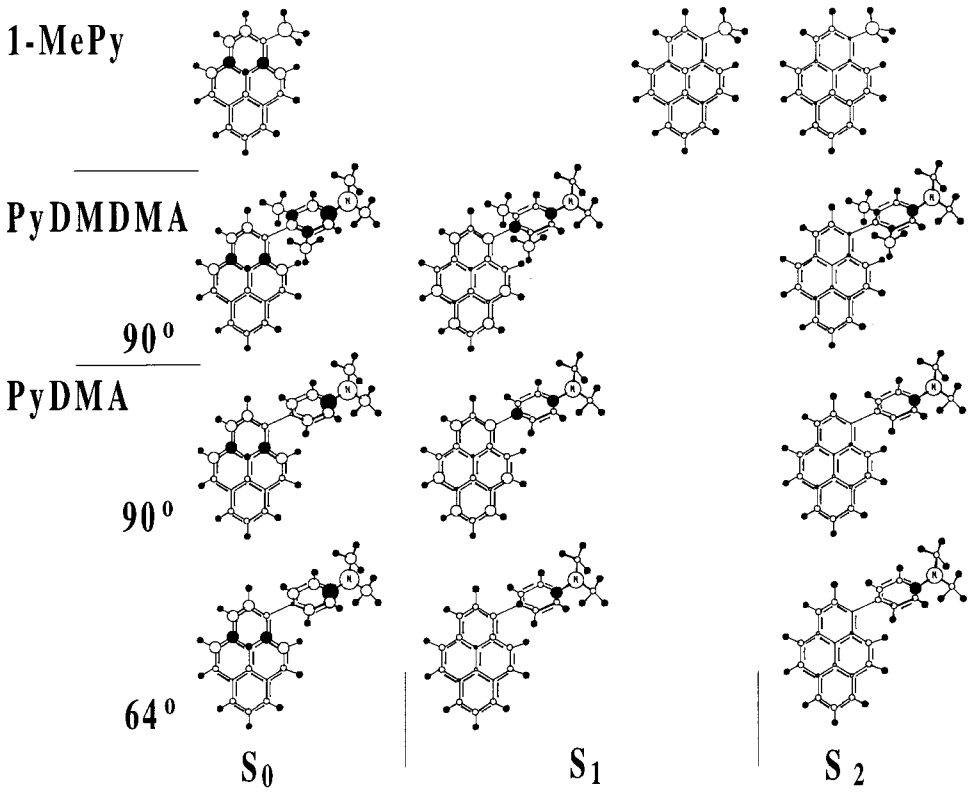

Figure 8. Mulliken population analysis of the ground and the first and second excited states of 1-MePy (top), PyDMDMA (middle), and PyDMA at two different configurations (bottom).

of negative charge. Depending on the size of the local charge the size of the circles changes between "no charge" (δ_{charge} = 0.000−0.001 au), "small" (δ_{charge} = 0.001−0.01 au), "medium" (δ_{charge} = 0.01−0.1 au), and "big size" (δ_{charge} = 0.1−0.5 au). In general, independent of electronic state or configuration, the amino nitrogen and the neighbored carbon at the phenylic moiety show a large polarization due to a negative and a positive charge center. In the ground state the pyrene moiety shows negatively and positively polarized components in the ring (two planes of nodes with respect to the electronic wave function). In the S_1 and S_2 states the charge polarization effects in the pyrene moiety are less pronounced compared to the ground state. In the S_1 CT state the charge distribution of pyrene decreases from −0.32 au at Θ(py−dma) = 64° to −0.64 au at Θ(py−dma) = 90° due to the twist between the pyrene and the DMA moiety. The charge center is mainly located at the peripheric carbon atoms of the pyrene moiety. The charge distribution of DMA just shows the opposite behavior, it increases from +0.32 au at Θ-(py−dma) = 64° to +0.64 au at Θ(py−dma) = 90°. The change of the dihedral angle has no significant influence on the molecular charge distribution in the ground state and the second excited state.

D. Statistical Vibrational Analysis of the Absorption Spectra and Lifetime Calculation. As the calculations of the preceding chapter suggest, the differences of the experimental lifetimes of PyDMA and PyDMDMA can more or less be understood as an effect of steric hindrance, electronic coupling, and the inductive effect of the methyl substitution, if one assumes that PyDMA does not tilt into a Θ(py−dma) = 90° conformation during the radiative photo process.

An alternative way of analyzing the process, which entirely relies on experimental data, is the statistical analysis of the absorption spectra/absorption coefficients as described in what follows. Assumption of this analysis is—like in the chapter before—that the absorption and emission processes lead to Franck−Condon states, which essentially preserve geometry.

To carry out such a statistical approach on the absorption coefficient or oscillator strengths of the absorption spectra, respectively, one first has to take into account the intramolecular motions, namely all the vibrations that contribute to the photophysics. Dealing with the intramolecular motions requires measurement of the vibrational spectra of the compounds and carrying out a normal-mode analysis. PyDMA has 126 vibrations, 61 of which are infrared active due to symmetry reasons. Because of the huge amount of vibrations and the complicated assignment we refer to a forthcoming publication on this topic for details.[39] In the infrared spectrum 49 vibrational bands have been observed in the spectral region from 600 to 3000 cm^{-1}. All bands could be assigned using a procedure described in detail in ref 26. Table 3 summarizes some measured representative PyDMA vibrations, namely stretching (R(CC), r(CH)) and bending vibrations (α(CCC), β(CCC), ϵ(CCC), τ(CCH)). The analysis is based on a geometry, where the torsional angle of pyrene and DMA is Θ(py−dma) ≃ 64°.

Furthermore, the vibrational spectrum has been simulated on the basis of DFT electronic structure calculations[34] with the 6-31G basis set and Becke's three-parameter functional with hybride character,[40] which mixes the Hartree−Fock exchange with a nonlocal correlation expressed by the LYP functional.[41,42] The maximal deviation of the calculated values from the measured vibrational band maxima was about 15%, as seen in Table 3. Since the used spectrometer only allowed the observation of vibrations with fundamental frequencies higher than 600 cm^{-1}, especially for the low-frequency vibrational modes, one has to keep in mind that the referred values stem from calculations and could slightly vary from the experimental values and thus this will influence all further calculated properties.

TABLE 3: Some Observed $\tilde{\nu}_{obs}$ and Calculated (DFT) Wavenumbers $\tilde{\nu}_{calc}$ and Boltzmann Factors *g* for Some Characteristic Vibrations and Low-Frequency Vibrations of PyDMA, PyMDMA, and PyDMDMA (See Also Text)

substance	band	$\tilde{\nu}_{obs}$/cm^{-1}	$\tilde{\nu}_{calc}$/cm^{-1}	*g*	activity
PyDMA	*r*(CH)	3045	3098	0.000	IR
	R(CC)	1610	1580	0.000	IR
	β(CCC)	1320	1369	0.002	IR
	α(CCC)	830	793	0.006	IR
	τ(CCH)	840	810	0.017	IR
	ϵ(CCC)	680	680	0.032	IR
	τ(NCH)		191	0.397	Ra
	Δ_{inv}(NCH)		172	0.436	Ra
	ϵ(CCC)		146	0.494	Ra
	δ(CH$_3$)		120	0.560	Ra
	τ(CCH)		119	0.563	Ra
	β_{wag}(NCH)		119	0.563	Ra
	ϵ(CCC)		99	0.638	Ra
	ϵ_{tors}(CNC)		40	0.828	Ra
	ϵ_{tors}(CCC)		10	0.948	IR
PyMDMA	ϵ_{tors}(CCC)		11	0.948	IR
PyDMDMA	ϵ_{tors}(CCC)		>80	>0.679	IR

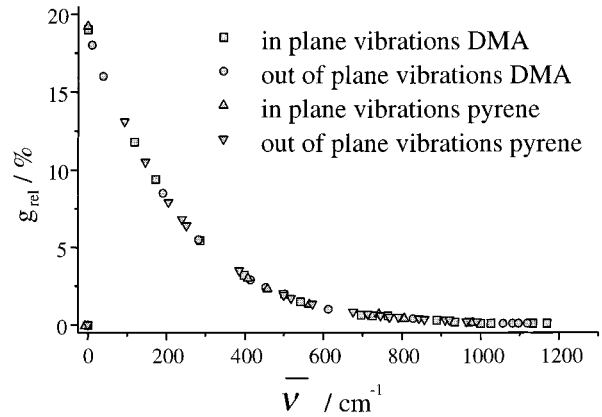

Figure 9. Boltzmann distribution function of PyDMA showing the large participation of low-frequency modes.

Taking into account all the calculated and measured vibrations and considering the corresponding Boltzmann distributions, which give indications of the population of the different vibrational states, it is obvious that particularly the low-frequency vibrational modes are well populated at room temperature. Figure 9 shows the large participation of all the low-frequency modes in PyDMA with relative Boltzmann factors up to 20% population for very low fundamental wavenumbers. The low-lying modes of PyDMA are also characterized in Table 3. These are the torsional motion between the methyl group and the amino moiety in DMA, τ(NCH), the inversion mode of the nitrogen, Δ_{inv}(NCH), the out-of-plane bending modes of pyrene itself (ϵ(CCC) at 146 and 99 cm^{-1}), the rocking motion of the CH_3 group, $\delta(CH_3)$, the out-of-plane bending mode of the benzene part in DMA, τ(CCH), the wagging motion in DMA, β_{wag}(NCH), the torsional motion between the amino moiety and the benzene moiety in DMA, ϵ_{tors}(CNC), and the torsional motion between pyrene and DMA, ϵ_{tors}(CCC). While all other normal modes are the same in the case of PyMDMA and PyDMDMA, the last mentioned IR active torsional mode ϵ_{tors}(CCC) increases from 10 to over 80 cm^{-1} in the case of PyDMDMA. To explain this change, results of chapter IIIC are anticipated. Since PyDMA is stabilized in a geometry characterized by the C_1 point group with benzene and pyrene moieties nearly lying in the same plane and a small barrier in the potential energy surface at a dihedral angle of 90° (see also chapter IIIC), the torsional vibrational motion of DMA against the pyrene moiety must be described as an anharmonic oscillation. In contrast PyDMDMA shows a local minimum at a dihedral angle of 90° (and has therefore to be treated in the C_s point group). This difference in the treatment of the vibrations is mainly reflected in the increase of the wavenumber of the ϵ_{tors}(CCC) mode from PyDMA to PyDMDMA. Also, the anharmonicity leads to torsional splittings (doublings) of the vibrational states (see Figure 10).

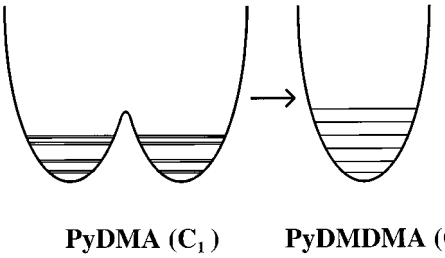

Figure 10. Torsional splitting and symmetry reduction: PyDMA (C_1 point group) compared to PyDMDMA (C_s point group).

If one assumes that from a statistical point of view (see the Boltzmann factors in Table 3) all these motions—not only the zero-point vibration—contribute to the lifetime of the charge-transfer fluorescence and excited-state lifetime, respectively, and that all these excited vibrational states are populated corresponding to the temperature of the sample and if one further assumes that the system works microscopically reversible in the limits of the Franck−Condon principle, the excited-state lifetime $\langle\tau\rangle$ can be calculated from the absorption spectrum.

The lifetime that corresponds to one vibronic transition, $S_u^{\upsilon'} \leftarrow S_n^{\upsilon''}$, namely the transition starting from one particular vibrational level υ' of one electronic state and ending in a vibrational level υ'' of another electronic state can be determined by

$$\tau_{S_u^{\upsilon'} \leftarrow S_v^{\upsilon''}} = \frac{3hN_A}{64\pi^4 n^2} \tilde{\nu}_{S_v^{\upsilon''} \leftarrow S_u^{\upsilon'}}^{-3} \int \epsilon(\tilde{\nu}_{S_v^{\upsilon''} \leftarrow S_u^{\upsilon'}})\, \mathrm{d}\tilde{\nu}_{S_v^{\upsilon''} \leftarrow S_u^{\upsilon'}} \quad (8)$$

A special case is the lifetime corresponding to a pure electronic transition $S_0^{\upsilon'=0} \leftarrow S_1^{\upsilon''=0}$ between two vibrational ground states in different electronic states. The term values of this transition are tabulated as $\tilde{\nu}(0,0)^{abs}$ in Table 4 and the corresponding lifetimes as $\tau^{abs}(0,0)$. These values have been determined directly from the absorption spectrum (transition $S_1^{\upsilon''=0} \leftarrow S_0^{\upsilon'=0}$) according to eq 8. Compared to the measured lifetimes $\langle\tau\rangle^{pc}$, the values tend to be too large.

Taking into account the Boltzmann distribution of all vibrations that are significantly populated at room temperature, the Einstein coefficients of the vibronic transitions have to be weighted with the vibrational Boltzmann distribution function, e.g., $A_{S_v \leftarrow S_u} = \sum_{\upsilon'} g_{uv,\upsilon''\upsilon'} A_{S_{\upsilon''} \leftarrow S_{\upsilon'}}$. Then, the overall vibrationally averaged lifetime can be rewritten as

$$\langle\tau\rangle = \frac{3hN_A}{64\pi^4 n^2} \frac{\langle\tilde{\nu}_{uv}^{-3}\rangle_A}{\int \epsilon(\tilde{\nu})\, \mathrm{d}\tilde{\nu}} \quad (9)$$

$$\langle\tilde{\nu}_{uv}^{-3}\rangle_A = \frac{\int \tilde{\nu}^{-3} \epsilon(\tilde{\nu}) L\, \mathrm{d}\tilde{\nu}}{\int \epsilon(\tilde{\nu}) L\, \mathrm{d}\tilde{\nu}} \quad (10)$$

Applying eq 9 leads to the calculated averaged lifetimes $\langle\tau\rangle^{abs}$ including all low-frequency modes that are thermally populated at room temperature and which are reported in Table 4. In general, the averaged lifetimes are smaller than the lifetimes

TABLE 4: Oscillator Strengths $f_{osc}^{abs}(0,0)$ and Lifetimes of 1-MePy, PyDMA, PyMDMA, and PyDMDMA Determined from Absorption Spectra and Measured by Photon Counting ($\langle\tau\rangle^{pc}$)[a]

substance	solvent	state	$\tilde{\nu}(0,0)^{abs}/cm^{-1}$	$f_{osc}^{abs}(0,0)$/	$\tau^{abs}(0,0)$/ns	$\langle\tau\rangle^{abs}$ (statistical)/ns	$\langle\tau\rangle^{pc}$/ns
1-MePy	hexOH	S_1	27 035	0.014	147	138	199
	ACN		26 037	0.015	140	135	196
PyDMA	*n*-hexane	S_1	25 776	0.3	14.0	3.9	2.5
	hexOH		25 866	0.3	13.8	3.8	3.7
	ACN		25 411	0.3	15.2	4.3	6.5
PyMDMA	*n*-hexane	S_1	25 979	0.05	44.5	12.0	4.4
	hexOH		25 924	0.05	44.7	12.1	8.3
	ACN		25 730	0.05	44.1	12.4	15.4
PyDMDMA	*n*-hexane	S_1	26 441	0.014	107	38.2	12.4
	hexOH		26 307	0.014	110	37.2	20.2
	ACN		26 507	0.014	110	37.9	24.4

[a] The data are compared with statistically weighted lifetimes $\langle\tau\rangle^{abs}$, which are determined from the absorption spectra by statistical analysis (see also text).

corresponding to the pure electronic transition and do not differ much from the measured values. The agreement between observed and calculated averaged lifetimes $\langle\tau\rangle^{abs}$ is satisfactory in the case of PyDMA. The differences for PyMDMA and PyDMDMA are mainly due to the higher uncertainty of the calculated absorption coefficients because of lack of absorption intensity. They may also be explained by the occurrence of a radiationless reaction channel or simply by the fact that the emitting state is not a Franck−Condon state with respect to the ground state, as is necessary for the applied approach (which means similar geometries).

Especially in PyMDMA and PyDMDMA none of the calculated lifetimes reflects the supposed solvent dependence of the experimental values, since the absorption spectra are not as much influenced by the solvent response as the emission spectra.

Since the torsional motion of the DMA moiety with respect to the pyrene plane is harmonic in the case of PyDMDMA and anharmonic in the case of PyDMA, the lowered fundamental wavenumber as well as the splitting of the states (Figure 10) contributes via the Boltzmann distribution function to the shortening of the lifetime of PyDMA compared to PyDMDMA.

The difference in the calculated emission lifetime of PyDMDMA ($\langle\tau\rangle^{abs} \simeq 40$ ns) to 1-methylpyrene ($\langle\tau\rangle^{abs} \simeq 150$ ns) and the measured lifetime $\langle\tau\rangle^{pc}$(PyDMDMA) $\simeq 20$ ns and $\langle\tau\rangle^{pc}$(1-MePy) $\simeq 200$ ns, respectively, can be explained by different species involved in the fluorescence process. In 1-methylpyrene an LE state is involved in the emission transition, whereas the emission in PyDMDMA starts from a CT state. The stronger allowed electronic transition of the CT of PyDMDMA leads to a shortening of the emission lifetime compared to the LE fluorescence of 1-methylpyrene. Furthermore, 1-methylpyrene resembles electronically more the D_{2h} point group of unsubstituted pyrene than PyDMDMA. In 1-methylpyrene, the nearly degenerate electronic states also contribute to the longer lifetime.

The oscillator strengths $f_{osc}^{abs}(0,0)$ of the electronic transitions of PyDMA, PyMDMA, and PyDMDMA are also summarized in Table 4. They reflect in physical quantities the transition probabilties that are qualitatively described in chapter IIIA. The oscillator strengths were calculated according to[37]

$$f^{osc}_{S_{u'}\leftarrow S_{v''}} = \frac{\mu_e c^2}{\pi e^2 N_A}\int \epsilon(\tilde{\nu}_{S_{v''}\leftarrow S_{u'}})\, d\tilde{\nu}_{S_{v''}\leftarrow S_{u'}} \qquad (11)$$

E. Pyrene-Specific Vibronic Coupling. In the case of PyDMA, Figure 3 shows that, in the region where the transition in the S_2 state crosses transitions of the vibrationally highly excited S_1 state (around 355 nm), the absorption band has parallel as well as perpendicular polarized components. Including the results of normal-mode analysis of the first excited state, as described in the section before, these lead to the suggestion that beyond the CT character of the first excited state a strong accidental vibronic coupling of the vibrational ground state of the second excited state and (exactly described) the first harmonic of a β(CCH) in-plane bending mode of the first excited state takes place. In pyrene itself the same kind of vibronic couplings are well-known since the 1970s.[24] There, polarization sensitive spectrosocopic measurements of pyrene in biphenyl and fluorene matrixes show an accidental vibronic coupling between the perpendicularly polarized β(CCH) (in-plane) bending mode of the perpendicularly polarized S_1 state and the parallel polarized vibrational zero-point level of the parallel polarized S_2 state.[24,43,44] Here, this means that the suggested vibronic coupling seen in PyDMA is introduced by the special peculiarities of the pyrene moiety. Since in PyDMA the coupling states have less pronounced CT character in the S_2 state and strongly pronounced CT character in the S_1 state, respectively, an excitation in this mixing area of the two states could lead to a special kind of electron transfer between the second excited state and the first excited (CT) state due to vibronic coupling.

The reader, who is interested in details of the theoretical features on how vibronic coupling can support electron-transfer processes and how to extract the information out of the absorption spectra, is referred to the Supporting Information, since a detailed treatment of this subject would be beyond the scope of this account. At least it shall be mentioned that within an adiabatic approach vibronic couplings can be treated similar to Fermi resonances and that vibronic coupling has a similar influence on intramolecular electronic energy redistribution like Fermi resonances on intramolecular vibrational energy redistribution.

IV. Conclusion

In this work three covalently linked donor−acceptor systems, PyDMA, PyMDMA, and PyDMDMA, have been studied using stationary IR absorption, UV (polarization) absorption and emission methods, and time-resolved photon counting. Though the only difference of these compounds is the methyl substitution on the DMA moiety, large differences in spectroscopic and kinetic properties could be found.

In the following the experimental characteristics of the CT state were discussed concerning the issues "twist movement as one preferred large amplitude motion", "statistical approach", and "pyrene-specific vibronic coupling".

First, the experimental data and their results have been compared with physical properties determined from ab initio

potential energy surfaces. The results of the ab initio calculations are in good agreement with the experimental data. It has been found that for all three systems the S_1 state has a high charge-transfer character and that this state is directly optically populated to different amounts.

A complete vibrational analysis of the systems was required for the kinetic statistical work. In general, the statistical analysis of the absorption spectra and lifetimes (based on IR measurements) independently lead to the same conclusion as the theoretical approach described in chapter IIIC, namely that the emission behavior of PyDMA can be satisfactorily explained from an emitting Franck−Condon state with similar geometry compared to the ground state, but less satisfying in the case of PyMDMA and PyDMDMA. The good agreement between experimental fluorescence lifetimes and lifetimes obtained from the statistical treatment of the absorption coefficients/oscillator strengths lead to the conclusion that (within the error of the experiments and the calculation) a sum of large amplitude motions, namely all low-frequency vibrations described in Table 3, contribute to the lifetime of the charge-transfer state. However in PyDMA, large amplitude motions are caused by highly anharmonic potential energy surfaces and lead to level splittings that characteristically influence the photodynamics. This influence is less pronounced in PyMDMA and diminished in the PyDMDMA system.

An accidental vibronic coupling between the S_1 (CT) state and the S_2 state with a bending mode as the mediating coupling mode is an additional characteristic feature of these systems and most pronounced in the case of PyDMA.

How vibronic couplings as a quantum mechanical phenomenon influence photophysical reaction paths and how different large amplitude motions contribute to CT properties and electron transfer is a fascinating field that requires more detailed experimental work implementing additional techniques. To understand more deeply the fast solvent response after the generation of the charge-transfer species, picosecond spectrostreak measurements have been carried out and provided valuable data and knowledge.[28] Transient absorption spectroscopy should also lead to a better understanding of the dynamics on the excited-state energy surfaces.[28] The work on the stationary and dynamic infrared and Raman properties in particular in the low-frequency range should be intensified.

On the theoretical side, more detailed calculations on the influence of vibronic couplings as intrinsic properties of the systems and the change of energy gaps due to the redox behavior of the attached substituents should be carried out. Using DFT as well as ab initio methods with larger basis sets as a first-principles approach should become easier with increasing computer power.

Acknowledgment. The authors thank B. Frederichs and H. Meyer for technical assistance and the members of the preparative organic chemistry group of the department (MPI) for the synthesis of the compounds. Financial support by the Deutsche Forschungsgemeinschaft through grant DFG-Sta 213/1-1 is gratefully acknowledged.

Supporting Information Available: Textual details of pyrene-specific vibronic coupling with supporting calculations and references, a table of coupling matrix elements, and figures showing a scheme of nonadiabatic transitions and the logarithm of the density of states as a function of G. This information is available free of charge via the Internet at http://pubs.acs.org.

References and Notes

(1) Dapprich, J.; Walter, N.; Salinque, F.; Staerk, H. *J. Fluoresc.* **1997**, *7*, 87 S.
(2) Petrov, N. Kh.; Kühnle, W.; Fiebig, T.; Staerk, H. *J. Phys. Chem. A* **1997**, *101*, 7043.
(3) Bourson, J.; Valeur, B. *J. Phys. Chem.* **1989**, *93*, 3871.
(4) Onkelinx, A.; Schweitzer, G.; De Schryver, F. C.; Miyasaka, H.; Van der Auweraer, M.; Asahi, T.; Masahura, H.; Fukumura, H.; Yashima, A.; Iwai, K. *J. Phys. Chem. A* **1997**, *101*, 5054.
(5) Okada, T.; Mataga, N.; Baumann, W.; Siemiarczuk, A. *J. Phys. Chem.* **1987**, *91*, 4490.
(6) Tominaga, K.; Walker, G. C.; Jarzeba, W.; Barbara, P. F. *J. Phys. Chem.* **1991**, *95*, 10475.
(7) Wiessner, A.; Kühnle, W.; Fiebig, T.; Staerk, H. *J. Phys. Chem. A* **1997**, *101*, 350.
(8) Onkelinx, A.; De Schryver, F. C.; Viaene, L.; Van der Auweraer, M.; Iwai, K.; Yamamoto, M.; Ichikawa, M.; Masahura, H.; Maus, M.; Rettig, W. *J. Am. Chem. Soc.* **1996**, *118*, 2892.
(9) Rotkiewicz, K.; Grabowski, R.; Krowczynski, A.; Kühnle, W. *J. Lumin.* **1976**, *12*, 877.
(10) Lippert, E.; Rettig, W.; Bonacic-Koutecky, V.; Heisel, F.; Miehe, J. A. In *Advanced Chemical Physics LXVIII*; Rice, S. A., Prigogine, I., Eds.; J. Wiley and Sons: New York, 1987.
(11) Rettig, W.; Lapouyade, R. In *Topics in Fluorescence Spectroscopy 4*; Lakowicz, J. R., Ed.; Plenum Press: London, 1994.
(12) Tominaga, K.; Walker, G. C.; Kang, T. J.; Barbara, P. F.; Fonseca, T. *J. Phys. Chem.* **1991**, *95*, 10475.
(13) Dey, J.; Warner, I. M. *J. Phys. Chem. A* **1997**, *101*, 4872.
(14) Wiessner, A.; Hüttmann, G.; Kühnle, W.; Staerk, H. *J. Phys. Chem.* **1995**, *99*, 14923.
(15) Dobkowski, J.; Waluk, J.; Yang, W.; Rulliere, C.; Rettig, W. *New J. Chem.* **1997**, *21*, 429.
(16) Herbich, J.; Kapturkievicz, A. *Chem. Phys.* **1993**, *158*, 143.
(17) Weller, A. Unpublished results.
(18) Dewar, M. J. S.; Mole, T. *J. Chem. Soc.* **1956**, *7*, 2556.
(19) Norman, R. O. C.; Thompson, G. A.; Waters, W. A. *J. Chem. Soc.* **1958**, *12*, 175.
(20) Parker, C. A. *Photoluminescence in Solution*; Elsevier: Amsterdam, 1968.
(21) Melhuish, W. H. *Proc. Conf. Natl. Bur. Stand.* **1972**, *378*, 138.
(22) Birks, J. B. *Photophysics of Aromatic Molecules*; J. Wiley and Sons Ltd.: London, 1970.
(23) Bree, A.; Kydd, R. A.; Misra, T. N.; Vilkos, V. V. B. *Spectrochim. Acta* **1971**, *27 A*, 2315.
(24) Bree, A.; Vilkos, V. V. B. *Spectrochim. Acta* **1972**, *27A*, 2333.
(25) Vala, M.; Szcepanski, J.; Pauzat, F.; Parisel, O.; Talbi, D.; Ellinger, Y. *J. Phys. Chem.* **1994**, *98*, 9187.
(26) Techert, S. Ph.D. Thesis; Georg-August-Universität: Göttingen, 1997.
(27) Thulstrup, E. W.; Michl, J. *Elementary Polarisation Spectroscopy*; VCH: New York, 1989.
(28) Techert, S.; Wiessner, A.; Schmatz, S.; Staerk, H. Submitted to *J. Phys. Chem. A.*
(29) Kirkwood, J. G. *J. Chem. Phys.* **1934**, *2*, 351.
(30) Lippert, E. *Z. Naturforsch.* **1955**, *10A*, 6512.
(31) McRae, E. G. *J. Phys. Chem.* **1957**, *26*, 562.
(32) Liptay, W. *Z. Naturforsch.* **1965**, *20A*, 1441.
(33) Beens, H.; Knibbe, H.; Weller, A. J. *J. Chem. Phys.* **1967**, *47*, 1183.
(34) Frisch, M. J.; Trucks, G. W.; Schlegel, H. B.; Gill, P. M. W.; Johnson, B. G.; Robb, M. A.; Cheeseman, J. R.; Keith, T.; Petersson, G. A.; Montgomery, J. A.; Raghavachari, K.; Al-Laham, M. A.; Zakrzewski, V. G.; Ortiz, J. V.; Foresman, J. B.; Cioslowski, J.; Stefanov, B. B.; Nanayakkara, A.; Challacombe, M.; Peng, C. Y.; Ayala, P. Y.; Chen, W.; Wong, M. W.; Andres, J. L.; Replogle, E. S.; Gomperts, R.; Martin, R. L.; Fox, D. J.; Binkley, J. S.; Defrees, D. J. anf Baker, J.; Stewart, J. P.; Head-Gordon, M.; Gonzalez, C.; Pople, J. A. *Gaussian 94*, Revision B.2; Gaussian Inc.: Pittsburgh, PA, 1995.
(35) Foresman, J. B.; Head-Gordon, M.; Pople, J. A.; Frisch, M. J. *J. Chem. Phys.* **1992**, *96*, 135.
(36) Wang, S.; Cai, J.; Sadygov, R.; Lim, E. C. *J. Phys. Chem.* **1995**, *99*, 7416.
(37) Herzberg, G. *Molecular Spectra and Molecular Structure, II. Infrared and Raman Spectra of Polyatomic Molecules*; Robert E. Krieger Publishing Co.: Malabar, FL, 1991.
(38) Tsubomura, H.; Mulliken, R. *S. J. Chem. Phys.* **1955**, *23*, 397.
(39) Techert, S.; Schmatz, S. Manuscript in preparation.
(40) Becke, A. D. *J. Chem. Phys.* **1993**, *98*, 5648.
(41) Lee, C.; Yang, W.; Parr, R. G. *Phys. Rev. B* **1988**, *37*, 785.
(42) Miehlich, B.; Savin, A.; Stoll, H.; Preuss, H. *Chem. Phys. Lett.* **1989**, *157*, 200.
(43) Klimova, L. A. *Chem. Phys. Lett.* **1970**, *4*, 537.
(44) Bree, A.; Vilkos, V. V. B. *Opt. Spectrosc.* **1963**, *14*, 185.